Study of Biological Activities of Magnetic Iron Oxide Nanoparticles Prepared by Co-Precipitation Method

[1]**Rania Hasan Hussein**[*], [2]**Ali A. Taha**, [1]**Oday Mahmood Abdulhusein**

[1]Applied Physics Division, Department of Applied Sciences, University of Technology, Baghdad – Iraq

[2]Biotechnology Division, Department of Applied Sciences, University of Technology, Baghdad – Iraq

Abstract

Iron oxides are the most common types of substances available in nature in various forms such as oxides, hydroxides and oxide-hydroxides, which obtained from various aqueous reactions. In the present study, iron oxide (Fe_3O_4) nanoparticles (NPs) had been synthesized using co - precipitation method and determined some biological activities. Iron oxide NPs had been characterized by spectrophotometry, X- Ray Diffraction (XRD) analysis and Field Emission Scanning Electron Microscopic (FE-SEM). The XRD analysis confirmed the purity and crystalline nature of fabricated NPs. In contrast, four biological activities of iron oxide NPs were determined. High removal of methylene blue pollutant dye (37.62 %) was observed when iron oxide NPs were used at 400 µg/ml within 48 hrs. Furthermore, iron oxide NPs revealed high inhibition zones of 27.5 and 30 mm, at 1000 µg/ml, toward Staphylococcus aureus and Escherichia coli respectively. The hemolysis activity of fabricated NPs is increases whenever concentrations increased. The lower hemolysis percentage of iron oxide NPs was (69.76%) when the NPs concentration was 250 µg/ml. Finally, cytotoxic activity was estimated against MCF- 7 cell line and normal cell line WRL68 by MTT assay. Significant and decrease in viability of (MCF-7 to 65.1%) when 400 µg/ml of iron oxide NPs was examined, while WRL68 viability was (75.03%).

1. Introduction

Metal oxide nanoparticles have exceptional properties that lead to great interest in some biological activities. Iron (Fe) is a transitional mineral and the backbone of the earth's crust appeared in different forms and magnetic properties, either as hematite (α-Fe_2O_3), magnetite (Fe_3O_4) or maghemite (γ-Fe_2O_3) [1, 2]. Magnetite is the most common types of substances available in nature in various forms such as oxides, hydroxides and oxide-

hydroxides, are obtained from various aqueous reactions (oxidation and reduction) [3]. Iron oxide NPs revealed more stable, superparamagnetic, biocompatible, and low toxicity compounds. They also have high stability in water when exposed to difficult conditions such as high temperature and high pH, and therefore their conjugation with biomolecules is very easy [4]. Moreover, synthesis methods of iron oxide NPs are extensively developed, like sol-gel, co-precipitation, thermal decomposition, and micro emulsion method [5]. On the other hand, iron oxide NPs have a high surface area to volume ratio, which gives the particles high binding ability and good dispersion in solution. Iron oxide nanoparticles have amazing magnetic properties and high biocompatibility that have attracted widespread interest in the biomedical field [1, 6]. In the present study, iron oxide NPs synthesized using co - precipitation process and then characterized by (UV-V) is spectroscopy, XRD and FE-SEM. The aim of this study is determining their compatibility, the ability to remove pollutant dye, hemolysis, antibacterial and antitumor activities had been investigated.

2. Experimental Work

2.1. Chemicals and Cells
Iron (II) chloride tetrahydrate ($FeCl_2.4H_2O_2$), Iron (III) chloride ($FeCl_3$), and Ammonium hydroxide (NH_4OH) were bought from Merck (India). Each solution was prepared to utilize deionized water. Bacterial isolates of *Staph, aureus* and *E. coli were* purchased from medical lab technique, Al Esraa university, Baghdad, Iraq, while MCF-7 and WRL68 cell lines were supplied by Sterllixir Biotech, industrial area, Bangalore, India.

2.2. Synthesis of Magnetic Iron Oxide NPs
The co-precipitation method was used for Fe^{3+}ions and Fe^{2+}ions to synthesize magnetic Fe_3O_4 nanoparticles in the presence of ammonium hydroxide solution (NH_4OH). The synthesis process was accomplished by mixing 4.58g of $FeCl_2.4H_2O$ with 8.93g $FeCl_3.6H_2O$ and dissolving them in an aqueous medium (80 mL). The solution was then heated at 80 °C with continues stirring. After heating, 10 mL of NH_4OH solution is added to the reaction solution. Crystal growth continuous for 30 minutes without changing the reaction conditions. Then the reaction solution is purified by washing it several times with distilled water drying in an oven at 50 °C [7].

2.3. Characterization of Iron Oxide NPs
(UV-Vis) is absorption spectra of iron oxide NPs were determined on UV-1800 spectrophotometer (Shimadzu, Kyoto, Japan). The crystal phase and particles size of the prepared sample was identified by X-ray technology (XRD-6000, Shimadzu) with Cu Kα source (wavelength of 1.54056 ˚A) at diffraction angle (2θ) from 20° to 80°. Furthermore, the morphology of the prepared iron oxide NPs can be identified by field emission scanning electron microscopy (Mira 3- TESCAN) and quickening voltage (20-30 kV).

2.4. Biological Activities Determination of Fe_3O_4 NPs
2.4.1. Removal of Methylene Blue
The adsorption activity of methylene blue dye has been studied. Various concentrations (5- 20 mg) of the prepared iron oxide NPs with methylene blue dye (50 mL, 40 mg L^{-1}) had been mixed. The reaction solution was mixed over a hot plate stirrer at different times 2-72 hr. and the process was repeated three times at room temperature. Finally, the removal percentage of methylene blue dye was measured using UV-Vis spectroscopy at wavelength 668 nm. Kinetics of adsorption was studied by analyzing adsorptive uptake of the dye color from the aqueous solution at different time intervals [8].

2.4.2. Antibacterial Activity
The well-diffusion technique was utilized in [9] with some modification. Fifty microliter of *E. coli,* and *S. aureus* cultures of 18-24 h (10^6 / CFU/ ml) growth were spread on the surface of sterilized Mueller-Hinton agar (Oxoid, England) poured in Petri plates. Wells were made and each well was packed with different concentrations of iron oxide NPs ranging from 250, 500, 750, and 1000 µg/ml DMSO. The plates were incubated at 37 °C for 24. DMSO was used as control. The antibacterial activity of (DMSO) used as control. The average of inhibition zones of duplicate treatment was determined in millimeters [9].

2.4.3. Hemolytic Activity Assay
Hemolytic activity of Fe_3O_4 NPs was established according to the procedure mentioned in [10] with some

modification. Briefly, 200 μL of the separated blood was mixed with 1600 μL of normal saline. Then, 200 μL of different concentrations of NPs (250, 500, 750, and 1000 μg / mL) were added to the diluted blood. The samples were incubated at 37°C for 1 h and centrifuged at 700 rpm for 5 min. Positive and negative control includes Distilled water and normal saline, respectively, were used for comparison. Sample absorbance was measured spectrophotometry at 541 nm and hemolysis percentage was estimated by utilizing the following equation 1 [10]:

$$\textbf{Hemolysis }(\%) = \textbf{A test sample} - \textbf{A}(-)\textbf{control} \backslash \textbf{A}(+)\textbf{control} - A(-)control\ x100 \quad \dots\dots(1)$$

Where, A: is the absorbance. The absorbance of positive and negative controls was found to be 1.764 and 0.048, respectively and A (-): is Negative control includes distilled water and A (+): is Positive control includes distilled water with normal saline.

2.4.4. Anticancer Activity
MCF-7 and WRL 68 cell lines were grown in RPMI-1640 medium (Sigma-Aldrich, USA) at 37 ^{o}C with 5% CO_2 in 96 - well flat bottom culture plates at density 1×10^4 cells /ml for 48 hrs. The cells were treated, in duplicate, with the concentrations of 20 - 400 μg/ml of NPs and incubated for 24 hrs. to determine the toxicity against examined cell lines. 10 μl of MTT solution was added to each well, and the plates were incubated for 4 hrs. at 37 ^{o} C. The media were then removed, and the remaining formazan crystals were dissolved in DMSO, and the absorbance was measured at 570 nm using an ELISA microplate reader to determine the toxicity, once with a tumor cell line and another with normal cells. The cytotoxicity percentage was calculated by the equation 2 [11]:

$$\textit{Growth Inhibition rate }\% (\textit{G. I}) = \frac{A-B}{A}\text{X } 100 \quad \dots\dots\dots(2)$$

A: an optical density of the control, B: an optical density of the treated sample.

3. Results and Discussion

3.1. Characterization of Iron Oxide NPs

3.1.1. UV-Vis Spectrophotometry Analysis
UV-Vis Spectroscopy is an analytical technique used to identify the absorbance of colloidal solutions and the optical properties of prepared compounds in a range of wavelengths (200-800) nm. Figure 1a, b shows the absorption spectrum of Fe_3O_4 NPs. The spectrum of Fe_3O_4 NPs shows continuous absorption along wavelengths and no strong absorption peaks observed. The results are similar to previous literature by Nagaraj *et al*.,[12] and Yen *et al*., [13]. Moreover, the band gap energy spectrum of Fe_3O_4 NPs had been determined, as exhibited in Figure (1 b). The optical band gap energy can be calculated from the Tauc's equation 3 [14]:

$$(\alpha h\nu)^2 = C(h\nu - E_g)^2 \quad \dots\dots\dots\dots(3)$$

Where, E_g is the band gap of the sample, h is blank constant, C is a constant, and α is the absorption coefficient. The gap energy is estimated by drawing $(\alpha h\nu)^2$ against the photon energy (hυ). It was found that the gap energy value of the Fe_3O_4 NPs up to 5.22 eV.
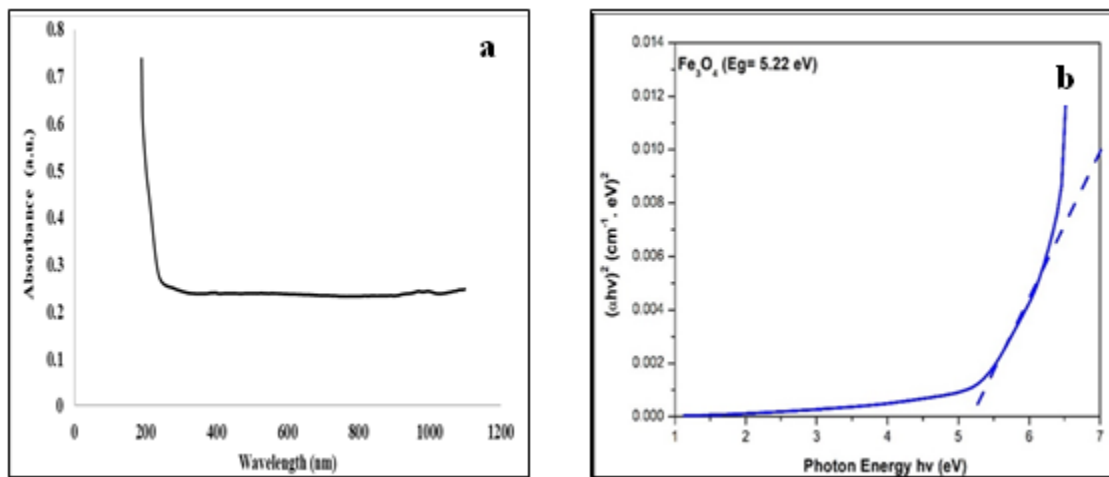
Figure 1: (a) UV-Vis Spectra properties of preparation Fe_3O_4 NPs and (b) the value of E_g using plot of $(\alpha h\upsilon)^2$ versus energy.

3.1.2 X-Ray Diffraction Analysis

XRD is an analytical technique utilized to identify the crystalline nature and particle size of prepared crystalline nanomaterials. Figure 2 represents the XRD patterns of Fe_3O_4 NPs. XRD patterns of Fe_3O_4 NPs exhibited the diffraction peaks of $2\theta = 30.77°$, $36.42°$, $43.48°$, $54.53°$, $56.78°$, and $62.28°$ corresponding to the hkl planes of (220), (311), (400), (422), (511) and (440), respectively as explained in Table 1. This point to the cubic spinel structure of Fe_3O_4 (JCPDS Card No: 19-629). The nonappearance of additional peaks in the spectrum indicates the high purity of the Fe_3O_4 NPs [15]. The average crystal size of Fe_3O_4 is 31.27 nm calculated from Debye Scherer's equation 4 [16]:

$$D = \frac{k\lambda}{\beta cos\theta} \dots\dots\dots\dots\dots\dots\dots (4)$$

Whereas D represents crystal size, θ is diffraction angle (deg.), λ is the X-ray wavelength (0.15056nm), k is a dimensionless shape factor (0.9), FWHM (β) is the full width at half maximum of the peak. The results are similar to previous literature [17, 18].
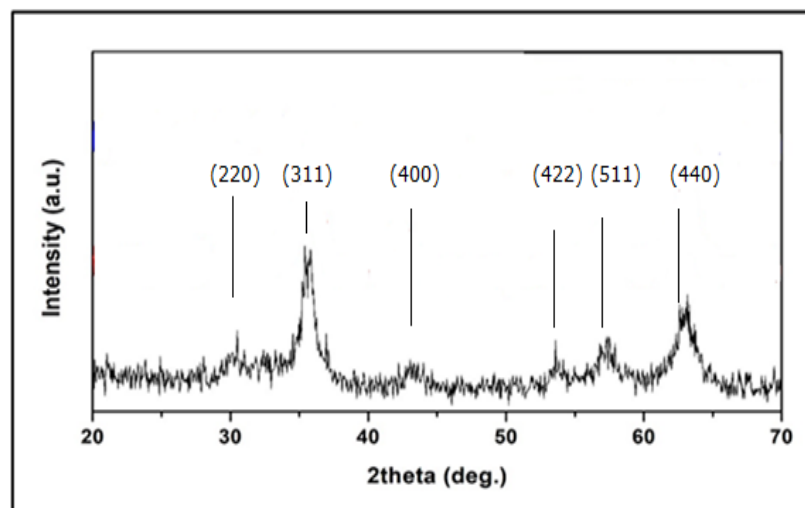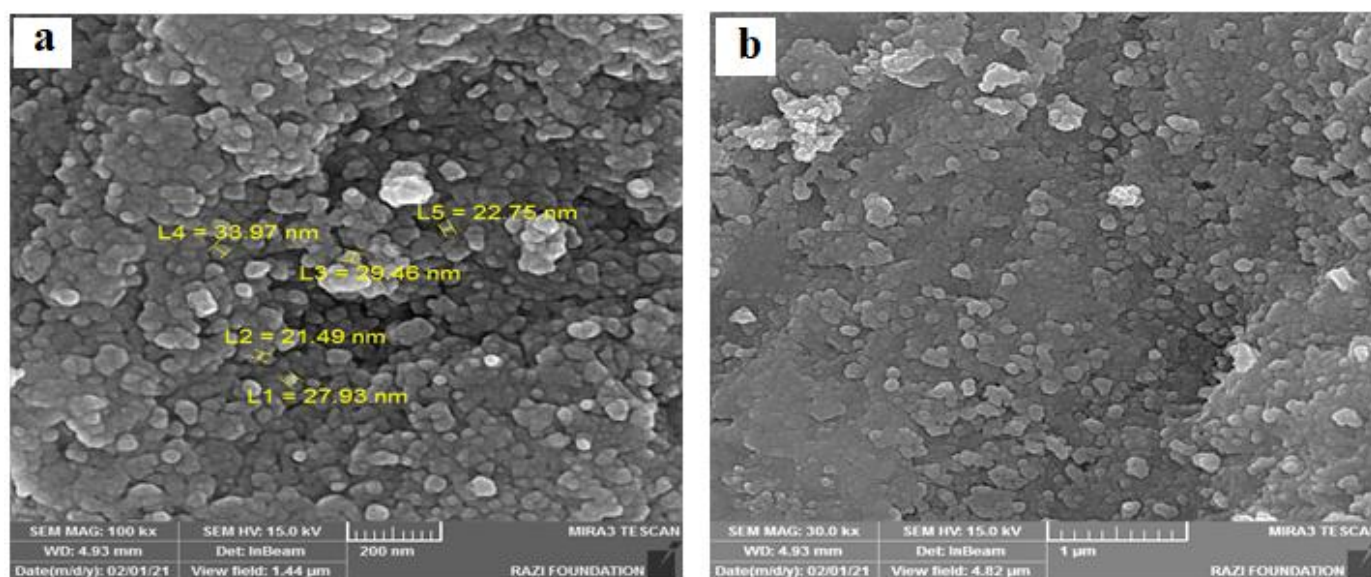

Figure 2: X- Ray diffraction spectra of Fe_3O_4 NPs.

Table 1: XRD analysis for Fe_3O_4 NPs.

2θ	Plane	FWHM	Crystalline Size D (nm)	d (A^o)
30.77	(220)	0.1858	31.27	2.3622
36.42	(311)	0.2841		2.3452
43.48	(400)	0.3735		2.0844
54.53	(422)	0.2944		1.6763
56.78	(511)	0.6880		1.6207
62.28	(440)	0.4420		1.4771

3.1.3. FE-SEM Images

FE-SEM is an analysis that provides information about surface morphology and particle size of the prepared samples. Figure 3 displays the FE-SEM analysis of iron oxide NPs. The microscopic images reveal the presence of spherical particles of different sizes and distribution. Also, an increase in the ratio of particle agglomeration was noticed due to the electrostatic interaction between the layers of nanoparticles.

Figure 3: FE-SEM images of Fe_3O_4 NPs with different magnifications (a) at scale bar = 200 nm and (b) scale bar =1 μm.

The average particle size is 27.12 nm, close to the crystal size calculated from the XRD diffraction analysis. The results show the formation of iron oxide nanoparticles, and this is in agreement with was previously published research [19]. On the other hand, EDS a diagnostic tool used to identify the elementary components of the chemical composition of the prepared sample. Figure 4 represents to EDS spectrum of iron oxide NPs with strong peak for the oxygen element and weak peaks for the Fe element were observed, indicating the formation of Fe_3O_4 compound. The results are identical to previous studies prepared by Saddam *et al,*.[9].
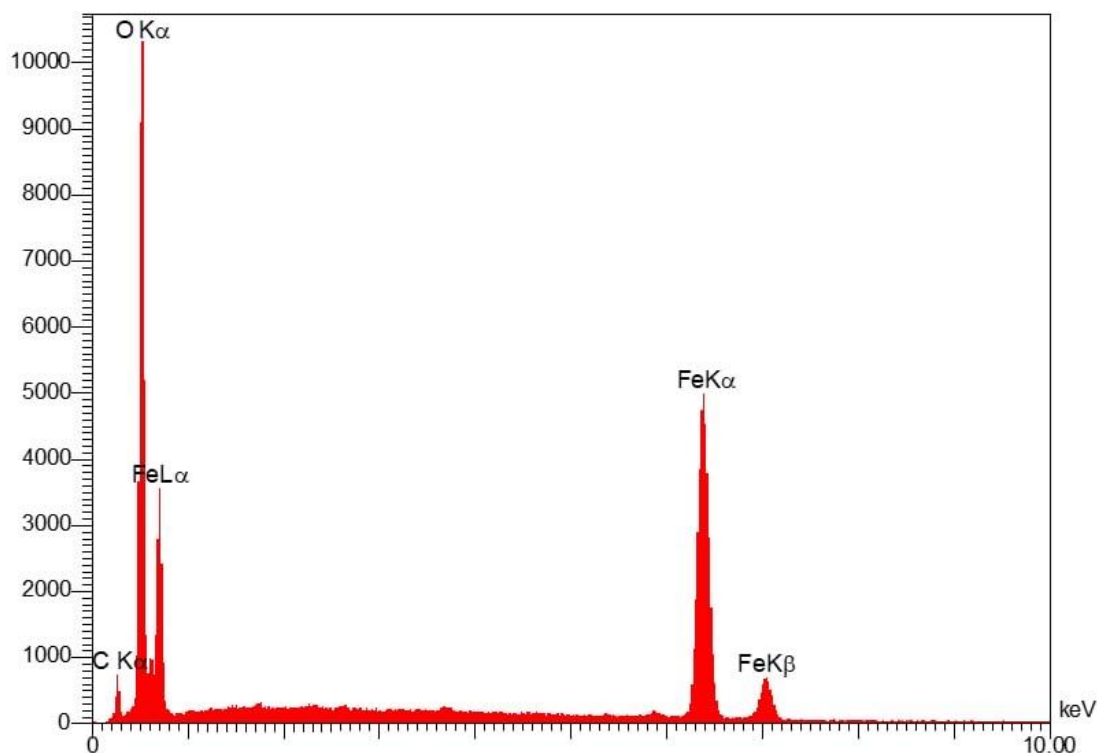
Figure 4: Energy dispersive spectroscopy of Fe_3O_4 NPs.

3.2. Biological Activities of iron oxide NPs

3.2.1. Removal of Methylene Blue (MB) Dye

Methylene blue had been used as pollutant dye model. The removal percentage of the dye had been estimated in the existence of iron oxide NPs in liquid phase. Absorbance of removed dye was measured in the existence of various concentrations of iron oxide NPs by spectrophotometer at 668 nm, within 48 hrs. at room temperature. High and significant removal of dye (37.62 %) was observed when iron oxide NPs was used at 400 µg/ml within 48 hr as shown in Figure 5. Most destruction and disruption of water ecosystems caused by untreated dye came from different industrial products, like textile, paper, and food processes. Further than their toxicity, most dyes are mutagenic and carcinogenic agents. Synthetic methylene blue is a cationic and aromatic dye used wildly in textile industry that cause skin damage and eyes allergy and other defects when ingested [20, 21]. Different remedying methods have been applied to remove methylene blue from water environments. The rapid and specific technique is the method of choice to isolate and concentrate the specific pollutant from water system. Magnetic nanoparticles represent easily and cheap prepared adsorbent material to remove contaminations [22]. On the other hand, although the reported advantages of nanoparticles, the toxicity of the iron oxide NPs need more to explore. Despite whether the applications were in vivo or in vitro, iron oxide NPs should be biocompatible and non-toxic. Moreover, surface area to volume of nanoparticles, size, shape, concentration of NPs, concentration of methylene blue, reaction temperature, type of coat, and pH effect dye removal [23]. Therefore, the results obtained in the study appeared low removal of methylene blue in contrast to results obtained by other studies [24].
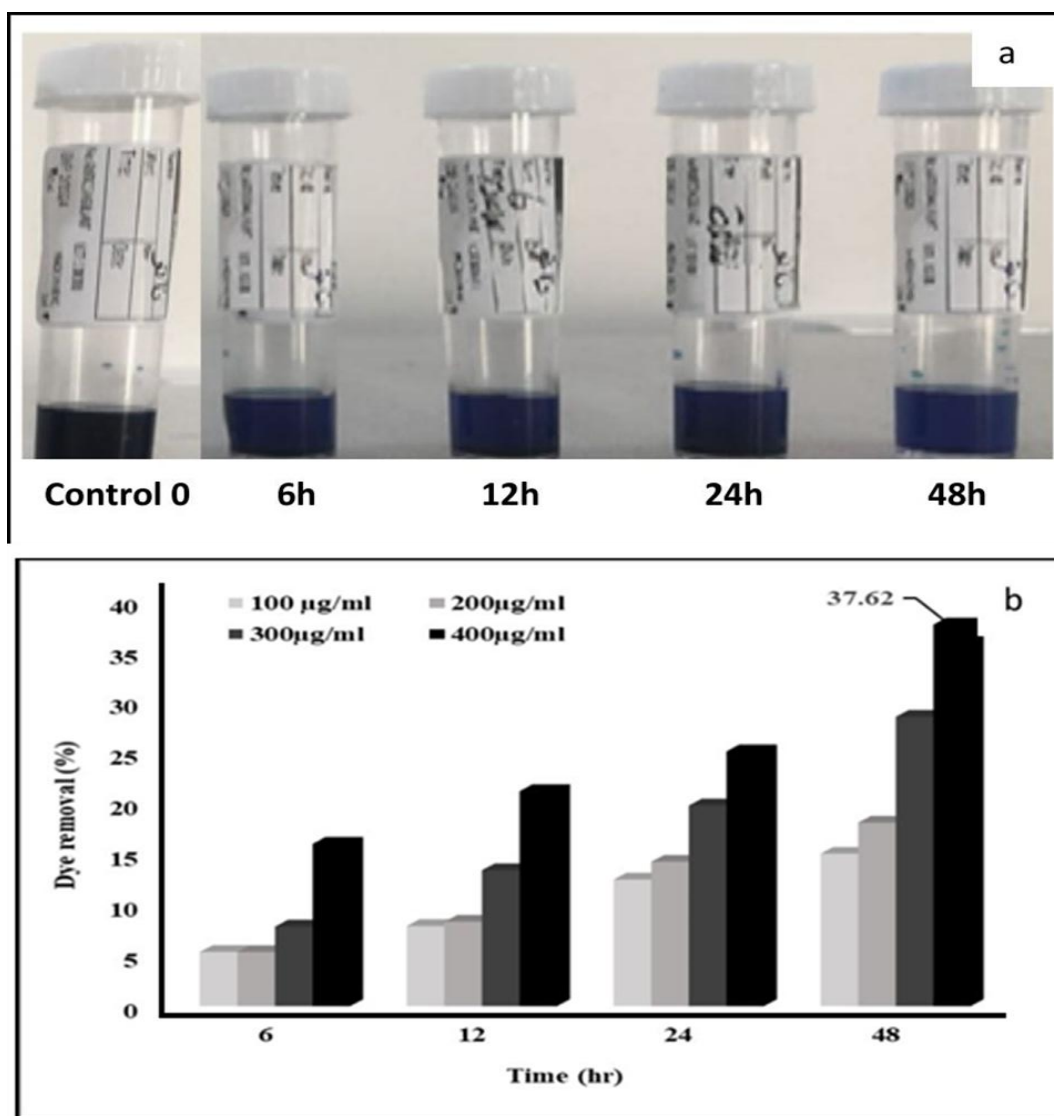
Figure 5: Methylene blue removal, (a) dye color changed using concentration 400 µg/ml of Fe_3O_4 NPs (b) Dye removal percent using different concentrations of Fe_3O_4 NPs, within 48 hr.

3.2.1 Antibacterial activity

Various concentrations of Fe_3O_4 NPs had been examined against *E. coli* (Gram negative) and *S. aureus* (positive bacteria. The well diffusion method was used to detected the antibacterial activity of Fe_3O_4 NPs on Muller Hinton medium within 24 hrs. at 37 °C. Results were expressed as mean ± standard error (SE) and values of $p<0.05$ were considered significant. The obtained results demonstrated that iron oxide NPs have antibacterial activity against both *E. coli* and *S. aureus* and the activity increases with an increase in concentration of nanoparticles. The oxide NPs, at 1000 µg/ml, revealed Highest and significant inhibition zones of 27.5 and 30 mm in diameter against *S. aureus* and *E. coli*, as shown in Figure 6. the other hand, investigation in many research had been done to explain the mechanism of iron oxide NPs antibacterial activity. One of the mechanisms referred to the interaction between opposite charge between the negative charge of bacterial surface and the potential positive charge of nanoparticles [25]. Due to the presence of positive charge on the surface of prepared iron oxide NPs [10,5], we think the attracted electrostatic led to an increase in the interaction between

prepared NPs and the examined bacteria. Furthermore, in the present study iron oxide NPs could be the source that produces reactive oxygen species (ROS) leading to the inhibition of bacterial growth.
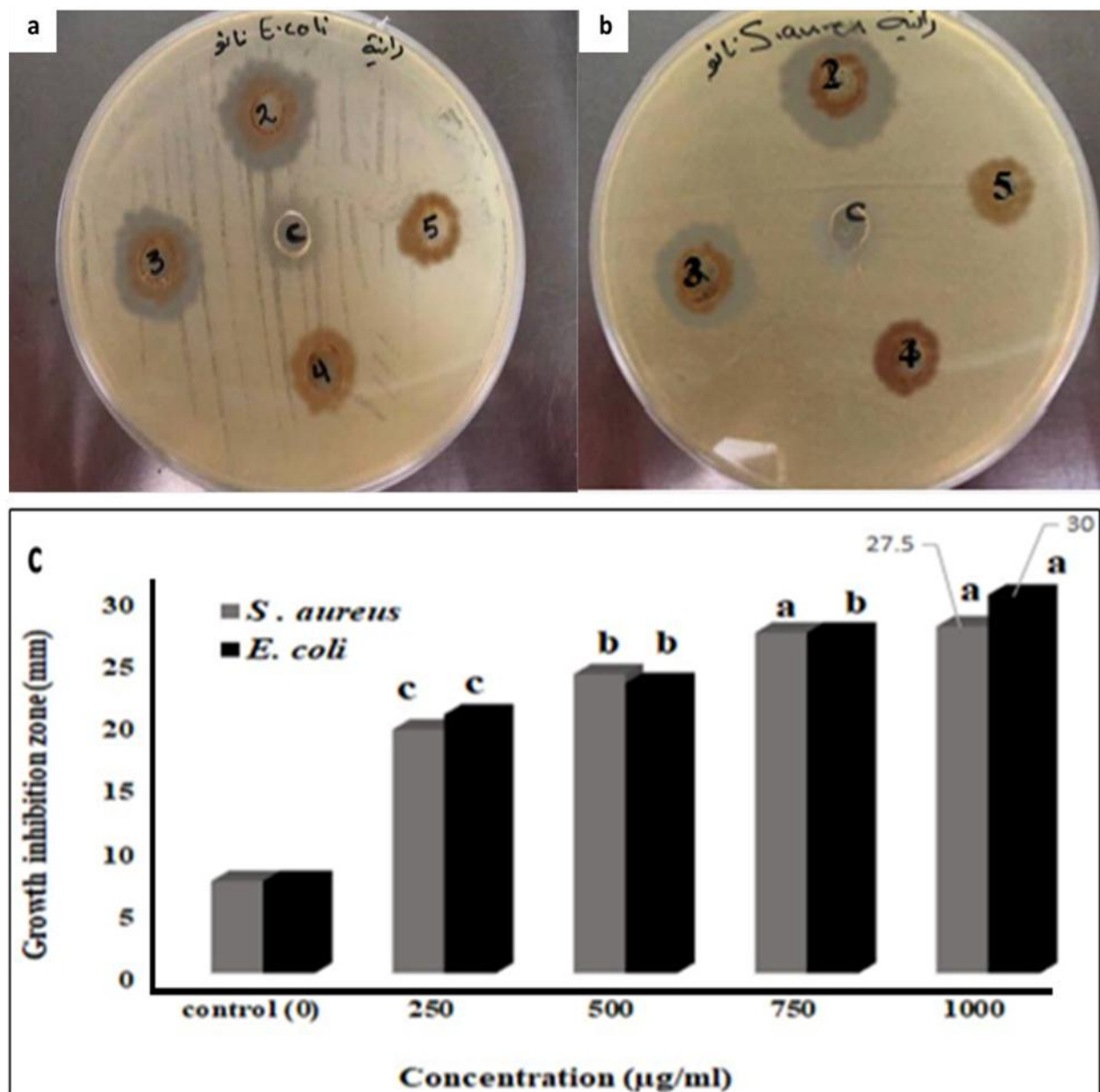

Figure 6: Inhibition Zone diameter around well filled with different concentrations of antibacterial Fe_3O_4 NPs (a) *E. coli* (b) *S. aureus* and (c) the Bar diagram of antibacterial Fe_3O_4 NPs.

3.2.3 Hemolysis Activity

The absorbance of human red blood cells corpuscles (RBC) lysis had been determined by spectrophotometer at 541 nm within one hour at 37 $^\circ$C. According to the standard ISO 10993-4 to evaluate materials and devices that compatible for blood cells, the hemolysis percentage should be less than 5 [27]. Different concentrations of iron oxide NPs were used to estimate their hemolysis activity, as shown in Figure 7. The hemolysis activity of iron oxide NPs is increasing whenever concentrations increased. Lower hemolysis percentages of iron oxide NPs

(69.76%) were observed at concentration of 250 µg/ml. Iron oxide NPs have wildly investigated and developed for biological and medical applications, but a few studies discussed the biocompatibility and less on their hemocompatibility. The concentration of iron oxide NPs and incubation time are other factors that affect hemolysis estimation in vitro. Hemolysis rates were found to be lower than 2 % for a low content 17.4 µg/ml and the highest 34.8 µg/ml of iron oxide NPs [28], while another study revealed maximum hemolysis (5.11%) was obtained at 125 µg/ml of iron oxide NPs [29]. On contrast study, the results indicate that the iron oxide NPs had non-hemolytic reaction at all examined concentrations up to 3.0 mg/ml [30].
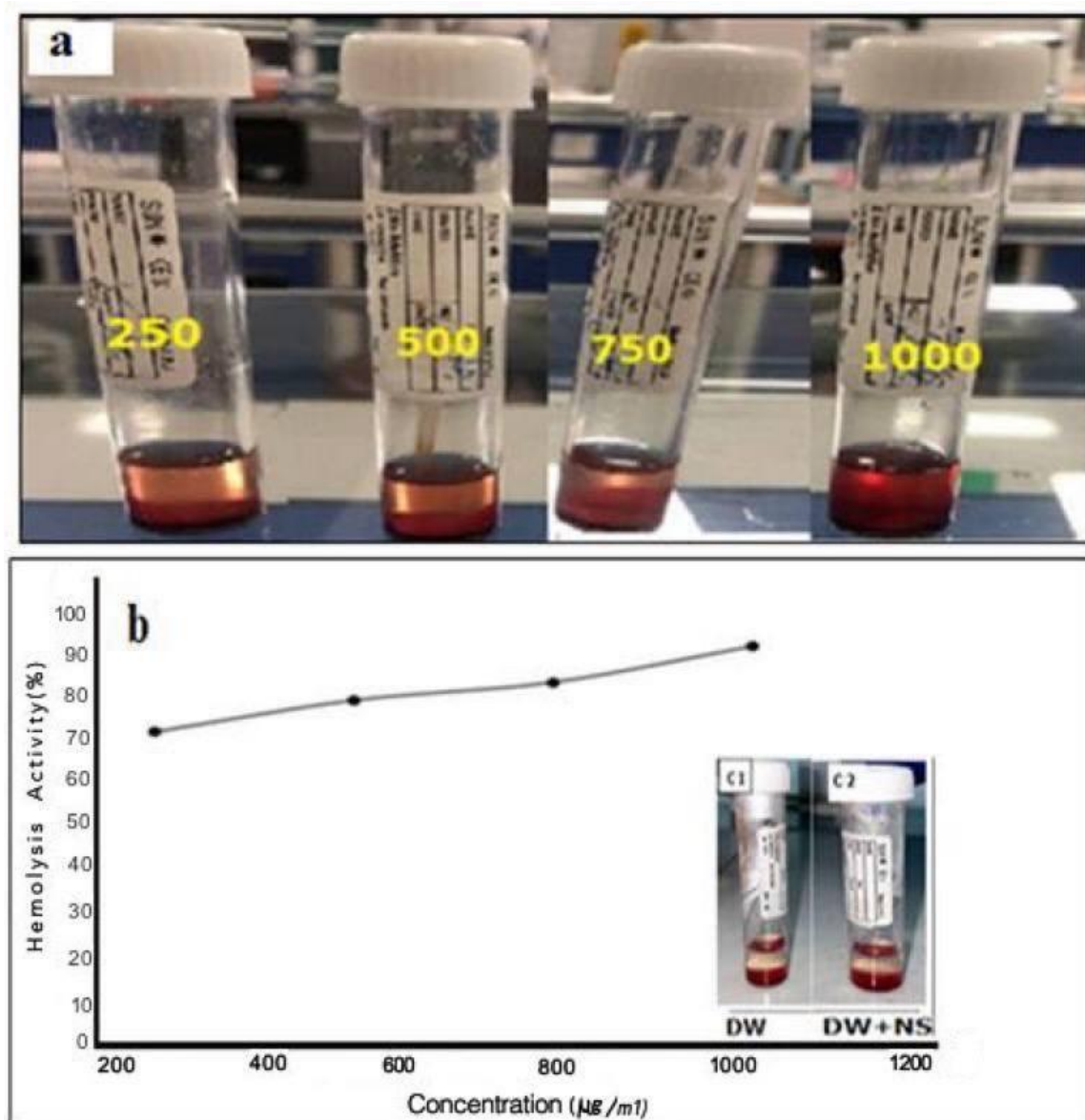

Figure 7: Hemolytic activity of Fe_3O_4 NPs (a) RBC lysis, (b) hemolysis percent by different concentrations (250-1000 µg/ml) of Fe_3O_4 NPs and (c) is 1: distilled water and 2: distilled water with normal saline.

3.2.4. Antitumor activity

Antitumor activity of different concentrations of iron oxide NPs were measured against MCF-7, as tumor cell line, and WRL68, as normal cell line. The MTT assay was used to determine cell viability after incubation of 25, 50 ,100, 200 and 400 µg/ml of NPs at 37 °C for 24 hr. in the presence of 5% CO_2. Significant and decreasing MCF- 7 viability reach 65.1% when 400 µg/ml of iron oxide NPs were examined, while the viability of WRL68 was 75.03%, as shown in Figure 8. Tumor can be treated either physically by radiation and hyperthermia or

chemically by intracellular entry of nanoparticles to induce ROS and most importantly, the apoptotic, programmed cell death, and necrotic, direct cell damage, in tumor cells populations. The apoptotic and necrotic populations in MCF-7 cells increased by 61% in 200 μg/mL of iron oxide NPs [31]. Moreover, treatment of DU145 and PC-3 cell lines with 100 µg/mL iron oxide NPs for 72 h resulted in significant inhibition of cell viability [32]. On the other hand, iron oxide NPs with 39 nm in size appeared a remarkable antitumor activity against renal tumor at concentration of 400 µg/ml [33-35].
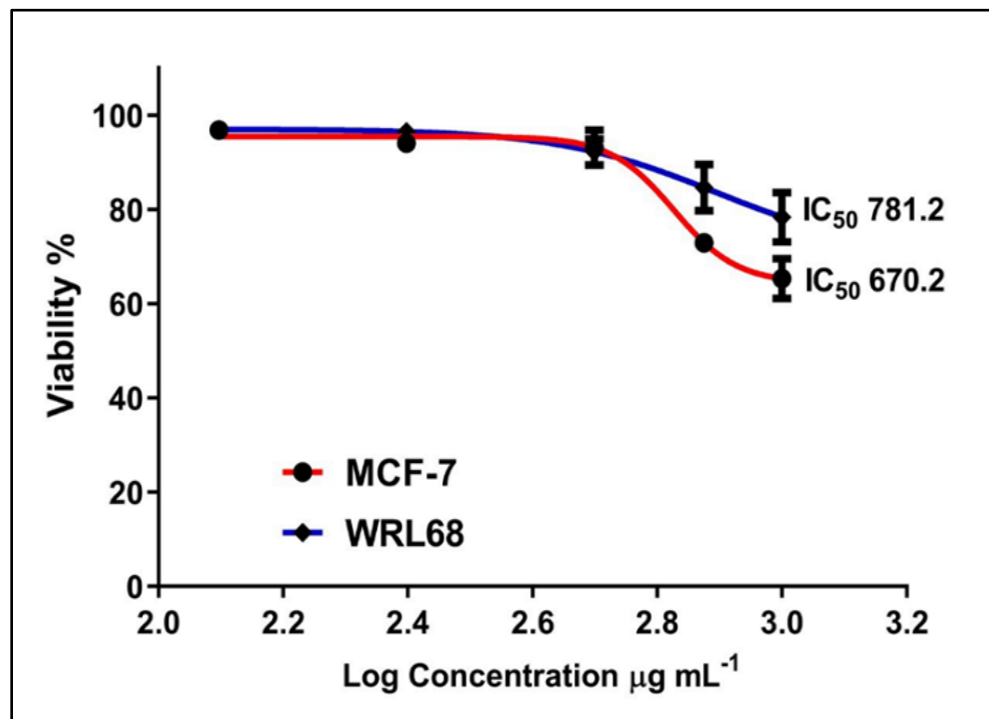

Figure 8: Antitumor activity of different concentrations Fe_3O_4 NPs determined by MTT assay against MCF and WRL68 cell lines.

4. Conclusions

The synthesis of iron oxide NPs by co - precipitation method revealed purity and crystalline nature by XRD. The FE-SEM images of iron oxide NPs reveal a homogeneous structure with spherical shapes closely related to each other. Iron oxide NPs can remove methylene, as a pollutant dye, but it needs more optimization. Moreover, the hemolysis activity of fabricated NPs is increasing whenever concentrations increased. On the other hand, it seems to be *E. coli* was more sensitive to iron oxide NPs than *S. aureus*. Finally, the iron oxide NPs revealed low toxicity against both MCF-7 and WRL 68, as tumor and natural cell lines, respectively.

Conflict of Interest

The authors declare that they have no conflict of interest.

References

[1] A. Ali, M.Z. Hira Zafar, I. ul Haq, A.R. Phull, J.S. Ali, A. Hussain, Synthesis, characterization, applications, and challenges of iron oxide nanoparticles, *Nanotechnology, science and applications*, vol. 9, p. 49, 2016.

[2] L. Machala, J. Tucek, R. Zboril, Polymorphous transformations of nanometric iron (III) oxide: a review, *Chemistry of Materials*, vol. 23, pp. 3255-3272, 2011.

[3] A.S. Teja, P.-Y. Koh, Synthesis, properties, and applications of magnetic iron oxide nanoparticles, *Progress in crystal growth and characterization of materials*, vol. 55, pp. 22-45,2009.

[4] A.V. Samrot, C.S. Sahithya, J. Selvarani, S. Pachiyappan, Surface-engineered super-paramagnetic iron oxide nanoparticles for chromium removal, *International journal of nanomedicine*, vol.14, p. 8105, 2019.

[5] M.O. Ansari, M. Ahmad, N. Parveen, S. Ahmad, S. Jameel, G. Shadab, Iron oxide nanoparticles-synthesis, surface modification, applications and toxicity: a review, *Materials Focus*, vol.6, pp 269-279,2017.

[6] O.A. Noqta, A.A. Aziz, I.A. Usman, M. Bououdina, Recent advances in iron oxide nanoparticles (IONPs): synthesis and surface modification for biomedical applications, *Journal of Superconductivity and Novel Magnetism*, vol.32, pp. 779-795,2019.

[7] S.A.M.K. Ansari, E. Ficiarà, F.A. Ruffinatti, I. Stura, M. Argenziano, O. Abollino, R. Cavalli, C. Guiot, F. D'Agata, Magnetic iron oxide nanoparticles: synthesis, characterization and functionalization for biomedical applications in the central nervous system, *Materials*, vol.12, p. 465,2019.

[8] A. Alinejad-Mir, A.A. Amooey, S. Ghasemi, Adsorption of direct yellow 12 from aqueous solutions by an iron oxide-gelatin nanoadsorbent; kinetic, isotherm and mechanism analysis, *Journal of Cleaner Production*, vol. 170, pp. 570-580,2018.

[9] S. Saqib, M.F.H. Munis, W. Zaman, F. Ullah, S.N. Shah, A. Ayaz, M. Farooq, S. Bahadur, Synthesis, characterization and use of iron oxide nano particles for antibacterial activity, *Microscopy research and technique*, vol.82, pp. 415-420,2019.

[10] Singh DK Graft AK. Graft copolymerization of 2- hydroxymethacrylate onto chitosan film and their blood compatibility. *J. Appl. Polym. Sci.* vol. 53, pp.1115-1121,1994.

[11] R.I. Freshney, Culture of animal cells: a manual of basic technique and specialized applications, John Wiley & Sons, 2015.

[12] N. Basavegowda, K.B.S. Magar, K. Mishra, Y.R. Lee, Green fabrication of ferromagnetic Fe_3O_4 nanoparticles and their novel catalytic applications for the synthesis of biologically interesting benzoxazinone and benzthioxazinone derivatives, *New Journal of Chemistry*, vol. 38, pp. 5415-5420,2014.

[13] Y.P. Yew, K. Shameli, M. Miyake, N. Kuwano, N.B.B.A. Khairudin, S.E.B. Mohamad, K.X. Lee, Green synthesis of magnetite (Fe_3O_4) nanoparticles using seaweed (Kappaphycus alvarezii) extract, *Nanoscale research letters*, vol.11, pp. 1-7,2016.

[14] K. Tharani, L. Nehru, Synthesis and characterization of iron oxide nanoparticle by precipitation method, Int *J Adv Res Phys Sci*,vol. 2,pp. 47-50,2015.

[15] S. Bao, K. Li, P. Ning, J. Peng, X. Jin, L. Tang, Highly effective removal of mercury and lead ions from wastewater by mercaptoamine-functionalised silica-coated magnetic nano-adsorbents: behaviours and mechanisms, *Applied Surface Science*, vol.393, pp. 457-466,2017.

[16] N. Budiredla, A. Kumar, S. Thota, J. Kumar, Synthesis and optical characterization of $Mg_{1-x}Ni_xO$ nanostructures, *International Scholarly Research Notices*, vol. 2012 p. 8, 2012.

[17] B. Gaihre, Y. Hee Lee, M. Seob Khil, H. Keun Yi, H. Yong Kim, In-vitro cytotoxicity and cell uptake study of gelatin-coated magnetic iron oxide nanoparticles, *Journal of microencapsulation*, vol. 28, pp. 240-247,2011.

[18] H. Zamani, B. Rastegari, M. Varamini, Antioxidant and anti-cancer activity of Dunaliella salina extract and oral drug delivery potential via nano-based formulations of gum Arabic coated magnetite nanoparticles, *Journal of Drug Delivery Science and Technology*, vol. 54, pp. 101278,2019.

[19] M.S.C. Kumar, V. Selvam, M. Vadivel, Synthesis and characterization of silane modified iron (III) oxide nanoparticles reinforced chitosan nanocomposites, *Engineering Science & Advanced Technology*, vol.2, pp. 1258-1263,2012.

[20] S. Sharma, A. Hasan, N. Kumar, L.M. Pandey, Removal of methylene blue dye from aqueous solution using immobilized Agrobacterium fabrum biomass along with iron oxide nanoparticles as biosorbent, *Environmental Science and Pollution Research*, vol.25, pp. 21605-21615,2018.

[21] S. Sharma, S. Tiwari, A. Hasan, V. Saxena, L.M. Pandey, Recent advances in conventional and contemporary methods for remediation of heavy metal-contaminated soils, 3 *Biotech*, vol.8, pp.1-18,2018.

[22] N. Besharati, N. Alizadeh, S. Shariati, Removal of cationic dye methylene blue (MB) from aqueous solution by Coffee and Peanut husk Modified with Magnetite Iron Oxide Nanoparticles, *Journal of the Mexican Chemical Society*, vol.62, pp.110-124,2018.

[23] N. Malhotra, J.-S. Lee, R.A.D. Liman, J.M.S. Ruallo, O.B. Villaflores, T.-R. Ger, C.-D. Hsiao, Potential toxicity of iron oxide magnetic nanoparticles: A review, *Molecules*, vol.25, p. 3159,2020.

[24] S. Thakur, P.P. Govender, M.A. Mamo, S. Tamulevicius, V.K. Thakur, Recent progress in gelatin hydrogel nanocomposites for water purification and beyond, *Vacuum*, vol. 146, pp. 396-408,2017.

[25] M. Arakha, S. Pal, D. Samantarrai, T.K. Panigrahi, B.C. Mallick, K. Pramanik, B. Mallick, S. Jha, Antimicrobial activity of iron oxide nanoparticle upon modulation of nanoparticle-bacteria interface, *Scientific reports*, vol.5, pp. 1-12,2015.

[26] Y. Abboud, T. Saffaj, A. Chagraoui, A. El Bouari, K. Brouzi, O. Tanane, B. Ihssane, Biosynthesis, characterization and antimicrobial activity of copper oxide nanoparticles (CoO NPs) produced using brown alga extract (Bifurcaria bifurcata), *Applied Nanoscience*, vol.4, pp. 571-576,2014.

[27] Q. Wang, M. Shen, T. Zhao, Y. Xu, J. Lin, Y. Duan, H. Gu, Low toxicity and long circulation time of polyampholyte-coated magnetic nanoparticles for blood pool contrast agents, *Scientific Reports*, vol. 5, pp. 1-8,2015.

[28] R.O. Rodrigues, M. Bañobre-López, J. Gallo, P.B. Tavares, A.M. Silva, R. Lima, H.T. Gomes, Haemocompatibility of iron oxide nanoparticles synthesized for theranostic applications: A high-sensitivity microfluidic tool, *Journal of Nanoparticle Research*, vol.18, pp. 1-17,2016.

[29] M. Imran, S. Riaz, S.M.H. Shah, T. Batool, H.N. Khan, A.N. Sabri, S. Naseem, In-vitro hemolytic activity and free radical scavenging by sol-gel synthesized Fe_3O_4 stabilized ZrO_2 nanoparticles, *Arabian Journal of Chemistry*, vol.13, pp. 7598-7608,2020.

[30] B. Macías-Martínez, D. Cortés-Hernández, A. Zugasti-Cruz, B. Cruz-Ortíz, E. Múzquiz-Ramos, Heating ability and hemolysis test of magnetite nanoparticles obtained by a simple co-precipitation method, *Journal of applied research and technology*, vol.14, pp. 239-244,2016.

[31] M.P. Vinardell, M. Mitjans, Antitumor activities of metal oxide nanoparticles, Nanomaterials, vol.5, pp.1004-1021,2015.

[32] K. Kojima, S. Takahashi, S. Saito, Y. Endo, T. Nittami, T. Nozaki, R.C. Sobti, M. Watanabe, Combined effects of Fe_3O_4 nanoparticles and chemotherapeutic agents on prostate cancer cells in vitro, *Applied Sciences*, vol.8, p.134, 2018.

[33] P. Nagajyothi, M. Pandurangan, D.H. Kim, T. Sreekanth, J. Shim, Green synthesis of iron oxide nanoparticles and their catalytic and in vitro anticancer activities, *Journal of Cluster Science*, vol.28, pp.245-257, 2017.

[34] M. A Al-Kinani, A. Haider Sharafaldin Al-Musawi., Study the Effect of Laser Wavelength on Polymeric Metallic Nanocarrier Synthesis for Curcumin Delivery in Prostate Cancer Therapy: In Vitro Study, *Journal of Applied Sciences and Nanotechnology*, vol. 1pp.43-5, 2021.

[35] N.N. Hussein, M., Khadum., Evaluation of the Biosynthesized Silver Nanoparticles Effects on Biofilm Formation, *Journal of Applied Sciences and Nanotechnology,* vol. 1, pp.23-31,2021.